PENETRATION FRACTURE OF ICE PLATE: 2D ANALYSIS AND SIZE EFFECT

By Yuan-Neng Li[1] and Zdeněk P. Bažant,[2] Fellow, ASCE

ABSTRACT: The problem of static penetration of an object through a sea ice plate is studied as a two-dimensional fracture problem using linear elastic fracture mechanics. The ice sheet floating on water is modeled as a thin elastic plate resting on Winkler's elastic foundation. The equilibrium equations are established by minimizing the potential energy approximated by finite differences in terms of nodal deflections. The growth of radial cracks is analyzed using the plate bending theory. The fracture process zone is assumed to be a point in the plane of plate. The maximum load is found to occur when circumferential cracks begin to form, which is governed by a strength criterion. As a refinement and extension of a previous idea, a theory of initial crack spacing is proposed to estimate the number of radial cracks formed during penetration. This theory can also explain the change of the failure mechanism, from failure by formation of circumferential cracks to failure by a conic crack. Particular attention is paid to the size effect. In addition to the size effect described by a simplified one-dimensional solution in a previous paper, the influence of the difference in the number of radial cracks on the size effect is discovered and analyzed.

INTRODUCTION

When an increasing upward or downward load is applied over a small area of ice plate floating on seawater, diffuse cracks first emerge at the other side of the ice plate. Subsequently, several radial cracks develop and propagate with increasing load. The maximum load is reached when circumferential cracks begin to form. After that the load decreases with increasing displacement and the plate wedges between the radial cracks are broken (Frankenstein 1963; Kerr 1975). Bažant and Li (1994) studied this problem using Nevel's (1959) narrow wedge-beam approximation, which is acceptable when the central angles of the wedges are sufficiently small. To solve the cases with larger wedge angles and to understand the limitations of the narrow wedge-beam approximation, a truly two-dimensional plate analysis must be conducted. To the best of our knowledge, there is no analytical solution for an infinite wedge plate with an arbitrary central angle resting on a Winkler's foundation.

The goal of the present study is to present a two-dimensional solution of the floating elastic wedge plate and use it to analyze fracture caused by penetrating objects. Commercial finite element programs for floating elastic plates seem unavailable, therefore, a variational form of the finite difference method is developed. The potential energy, approximated by finite differences, is minimized with respect to nodal deflections. Since regular meshes can be used with a polar coordinate system, the finite difference method appears to be simpler than the finite element method. The finite difference

[1]Res. Sci. in the Rank of Asst. Prof., Dept. of Civ. Engrg., Northwestern Univ., Evanston, IL 60208.

[2]Walter P. Murphy, Prof. of Civ. Engrg. and Mat. Sci., Northwestern Univ., Evanston, IL.

Note. Discussion open until December 1, 1994. To extend the closing date one month, a written request must be filed with the ASCE Manager of Journals. The manuscript for this paper was submitted for review and possible publication on January 11, 1993. This paper is part of the ***Journal of Engineering Mechanics***, Vol. 120, No. 7, July, 1994. ©ASCE, ISSN 0733-9399/94/0007-1481/$2.00 + $.25 per page. Paper No. 5407.

method has been used to solve plate problems [e.g. Selvadurai (1979)]; however, its classical form does not seem very suitable for the present problem.

With the variational principle, the static boundary condition is taken care of automatically and the matrix of equilibrium equations is symmetric, which yields considerable savings in computational effort. By using polar coordinates, the wedge can be treated as a rectangular region, which means that the geometric shape of the wedge can be modeled exactly, and the coding itself becomes much easier. The finite difference method based on a variational principle is a well-documented numerical approach [e.g. Forsythe (1960) and Hall (1990)]. Most applications are for the second-order partial differential equations. After this paper was submitted, one of the reviewers brought our attention to the work by Bushnell (1973), who used a similar variational finite difference method to solve various problems with shell structures.

The second goal is to analyze the fracture process two-dimensionally, determine the angular spacing and growth of the radial cracks, establish the relation between the plate thickness and the number of radial cracks, and, most importantly, clarify the size effect. Since the ice sheet may fail by a conic crack under the load, which is obviously a three-dimensional phenomenon, we will also attempt to provide some information on this type of failure.

VARIATIONAL PRINCIPLE AND ITS FINITE DIFFERENCE APPROXIMATION

Consider an ice plate [Fig. 1(*a*)] with polar coordinates (r, θ), floating on water and subjected to a vertical load P that is uniformly distributed along the circumference of a circle with radius a_0. Based on observations, it is assumed that the load produces n radial cracks of equal length a from the center, forming plate wedges of equal angles $\varphi_n = 2\pi/n$. The seawater, of unit weight ρ, acts exactly as an elastic (Winkler-type) foundation, because the buoyancy is exactly proportional to deflection. We assume that the

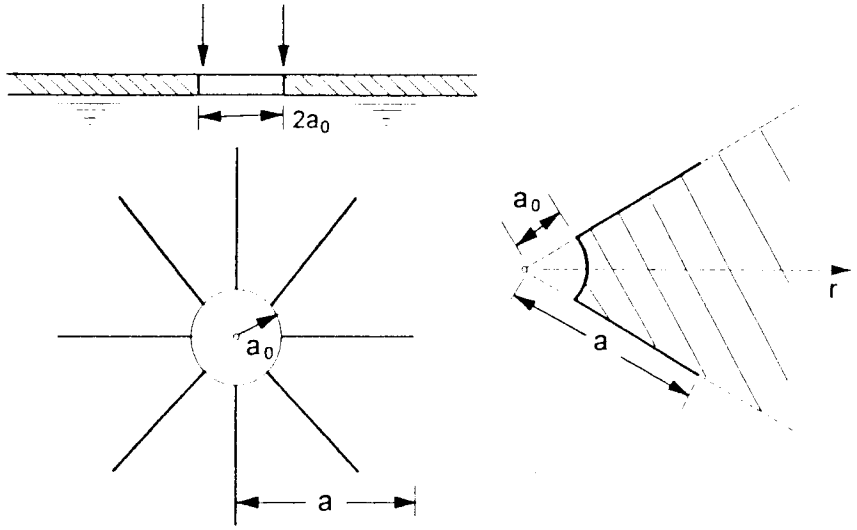

FIG. 1. (*a*) Floating Ice Sheet Subjected to Vertical Load; (*b*) Wedge Geometry

deflections are not so large that water could flood the top of the plate when it deflects downward, or the plate would not be lifted off of the water surface when it deflects upward.

Let $D = EI/(1 - \nu^2)$ be the plate stiffness, $I = h^3/12$ the moment of the inertia, and h = thickness of the plate, E = Young's modulus, and ν = Poisson's ratio. The expression $L = (D/\rho)^{1/4}$, which we will call the plate decay length, represents a basic characteristic of the plate-foundation system. To avoid the intrinsic singularity of the axisymmetric solution in the center, the material within the loaded circle is considered to be removed and load P is considered to be uniformly distributed along the circle $r = a_0$. As shown by Bažant and Li (1994), the removal of the material has a negligible effect on the maximum negative moment if $a_0/L \ll 1$. The surfaces of the radial cracks are assumed to be free, that is, the radial cracks are assumed to transmit no bridging moments and shear forces, which means we assume linear elastic fracture mechanics (LEFM) is applicable. Because the plate-bending theory requires the normals to remain straight, we must inevitably assume the fracture-process zone to be concentrated in one normal associated with one point. In reality, the fracture spreads gradually across the plate thickness, but this cannot be captured by two-dimensional analysis. Although the wedge is actually infinite, the radial length of the wedge is considered to be finite and is taken as $r = a_1 = 6.5L$, because the deflections are negligible for $r > 3L$ when only a small central region is loaded. The far side of the wedge can be treated as a free boundary. The behavior of the plate is assumed to be symmetric with respect to each radial crack and to the axis of symmetry of each wedge; therefore, only one-half of the wedge needs to be analyzed.

Introducing a nondimensional radial coordinate $x = r/L$, and substituting $\alpha = a/L$; $\alpha_0 = a_0/L$; and $\alpha_1 = a_1/L$, the potential energy Π of the wedge [Fig. 1(*b*)] can be expressed in a nondimensional form as

$$\Pi^* = \frac{\Pi}{\rho L^2} = \int_{\alpha_0}^{\alpha_1}\int_0^{\varphi_n/2}\left\{\frac{1}{2}\left(\frac{\partial^2 w}{\partial x^2} + \frac{1}{x}\frac{\partial w}{\partial x} + \frac{1}{x^2}\frac{\partial^2 w}{\partial \theta^2}\right)^2 + (1-\nu)\left[\left(\frac{1}{x}\frac{\partial^2 w}{\partial x \partial \theta} - \frac{1}{x^2}\frac{\partial w}{\partial \theta}\right)^2 - \left(\frac{\partial^2 w}{\partial x^2}\right)\left(\frac{1}{x^2}\frac{\partial^2 w}{\partial \theta^2} + \frac{1}{x}\frac{\partial w}{\partial x}\right)\right]\right\} x\, d\theta\, dx + \int_{\alpha_0}^{\alpha_1}\int_0^{\varphi_n/2}\frac{1}{2}w^2 x\, d\theta\, dx - \int_0^{\varphi_n/2}\frac{PL^2}{2\pi D}w\, d\theta \tag{1}$$

It should be noticed that the load P represents the total force applied on the ice sheet. The integrals corresponding to the boundary conditions along radial lines are deliberately neglected. Since along the radial lines of symmetry and of the extension of radial cracks we have zero Kirchhoff shear, while the slope in the θ-direction must be zero due to symmetry, the integral is zero. On the other hand, both the normal moment and Kirchhoff shear force are zero along the radial crack surface. Therefore the boundary integral in (1) vanishes along all the radial boundaries.

For a generic internal node, the integration will be carried out on a cell shown as the shaded area in Fig. 2(*a*). With the local node numbering defined in Fig. 2(*b*), the derivatives in the integrand can be approximated with second-order accuracy in h by finite difference expressions as follows:

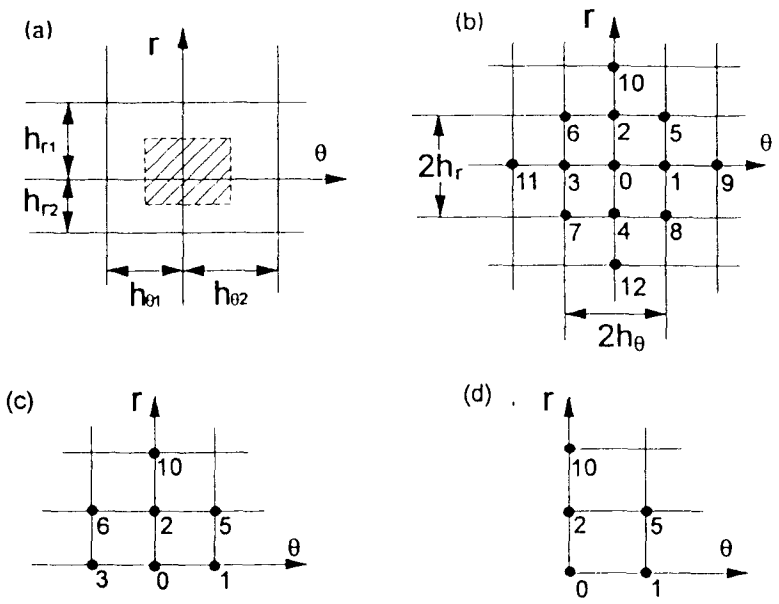

FIG. 2. (*a*) Geometric Definition of Mesh; (*b*) Local Node Numbering; (*c*) Generic Boundary Node; (*d*) Corner Node

$$\frac{\partial^2 w}{\partial x^2} \approx \frac{1}{h_r^2}\left[\lambda_1 w_2 - (\lambda_1 + \lambda_2) w_0 + \lambda_2 w_4\right] \tag{2a}$$

$$\frac{\partial^2 w}{\partial \theta^2} \approx \frac{1}{h_\theta^2}\left[\mu_1 w_1 - (\mu_1 + \mu_2) w_0 + \mu_2 w_3\right] \tag{2b}$$

where $h_r = (h_{r1} + h_{r2})/2$ = average nodal spacing along x-axis (the non-dimensional r-axis, $\lambda_1 = h_r/h_{r1}$ and $\lambda_2 = h_r/h_{r2}$; $h_\theta = (h_{\theta 1} + h_{\theta 1})/2$; $\mu_1 = h_\theta/h_{\theta 1}$; and $\mu_2 = h_\theta/h_{\theta 2}$. For the mixed second-order derivative and all first-order derivatives, central finite difference approximations (which are not exactly of second-order accuracy if the nodal spacings are unequal) are applied

$$\frac{\partial^2 w}{\partial x \partial \theta} \approx \frac{1}{4 h_r h_\theta}\left(w_5 - w_6 + w_7 - w_8\right) \tag{2c}$$

$$\frac{\partial w}{\partial x} \approx \frac{1}{2h_r}\left(w_2 - w_4\right) \tag{2d}$$

$$\frac{\partial w}{\partial \theta} \approx \frac{1}{2h_\theta}\left(w_1 - w_3\right) \tag{2e}$$

The foregoing approximations are valid only for the internal nodes. For the boundary nodes, a symmetric central finite difference approximation would become difficult because three of the nodes would fall out of the domain of the wedge. Although fictitious external nodal values could be introduced, they would have to be solved from the boundary conditions, making the formulation cumbersome for programming. In this paper, single-sided finite difference approximations, which have only first-order accuracy

(even for a uniform mesh), are used. For a generic node on boundary $x = \alpha_0$ [Fig. 2(*c*)] the second-order partial derivatives may be approximated as

$$\frac{\partial^2 w}{\partial x^2} \approx \frac{1}{h_r^2}(\lambda_1 w_{10} - (\lambda_1 + \lambda_2)w_2 + \lambda_2 w_0) \tag{3a}$$

$$\frac{\partial^2 w}{\partial x \partial \theta} \approx \frac{\lambda_2 \mu_2}{h_r h_0}(w_5 - w_2 + w_0 - w_1) \tag{3b}$$

In these approximations the central difference approximation with respect to θ is preserved. For the corner nodes [Fig. 2(*d*)], asymmetric finite difference approximations are used, e.g.

$$\frac{\partial^2 w}{\partial x \partial \theta} \approx \frac{\lambda_2 \mu_2}{h_r h_0}(w_5 - w_2 + w_0 - w_1) \tag{4}$$

Now we substitute these finite difference approximations into the integrand of the potential energy expression. The potential energy density in each integration cell of the mesh (the shaded area) is a quadratic function of the nodal deflections w_i, which also contains x as a variable in the expression. To carry out the area integration, Gaussian quadrature is employed to take care of the x variable. Six sampling points for the Gaussian quadrature seem to give sufficient accuracy. The integrand is constant in θ-direction, thus no special treatment is needed except that a proper coordinate incremental length h_0 must be multiplied to the results.

To find the equilibrium solution from the potential energy approximation, it is necessary that the partial derivative with respect to any nodal deflection w_i be zero. This yields a system of linear algebraic equations

$$[\mathbf{A}]\{\mathbf{W}\} = \{\mathbf{F}\} \tag{5}$$

where $\{\mathbf{W}\}$ = vector of the nodal displacements; $\{\mathbf{F}\}$ = vector of the applied load; and $[\mathbf{A}]$ = corresponding stiffness matrix. Because it is defined by minimization of the potential energy, $[\mathbf{A}]$ must be symmetric.

Note that, in deriving (5), no kinematic boundary condition has yet been taken into account. The condition of symmetry requires that the boundary rotation be zero. To implement it, (5) must be modified before $\{\mathbf{W}\}$ can be solved. The zero-rotation condition can be approximated as $w_0 = w_3$, where the local nodal numbering is used according to Fig. 2(*b*) and the plate is assumed to be placed to the left of the r-axis. Substituting this equation into (5) results in combining the columns corresponding to w_0 and w_3. To keep the symmetry, the corresponding two rows should also be combined.

DISTRIBUTIONS OF DEFLECTION AND MOMENTS

Because the deformation is distributed very inhomogeneously between α_0 and α_1, the mesh is nonuniform along the x-axis. Specifically, because the deformation varies rapidly in the range $x < 3$, the mesh is so designed that for small x-values the nodal spacing is smaller. In addition, the radial crack front coincides with one of the nodes so that the radial crack length is reproduced exactly. The displacement solution may be represented in the form

$$w(x, \theta) = \tilde{P}F(x, \theta; \alpha_0, \alpha); \quad \tilde{P} = \frac{PL^2}{2\pi D} \tag{6a,b}$$

where $\bar{P} = P/$ nondimensional load; and F (which has the same dimension as w) = displacement function to be found. The distributions of displacement as well as moment is calculated under the assumption that $\bar{P} = 1$.

The displacement field is examined in two perspectives. First, it is compared with the previously obtained narrow wedge-beam solution (Bažant and Li 1994). For this purpose, an average deflection is defined along each circumferential arc. The comparison is shown in Fig. 3 for the case where $\alpha_0 = 0.1$ and the radial crack length $\alpha = 3$. According to Bažant and Li (1994), the maximum nondimensional radial crack length that an applied load P can produce is about 2. Therefore, by selecting α 3 the wedge can be practically considered the same as a wedge with infinite length. When the number n of radial cracks is increased, the wedges become softer, and the solution is seen to converge. However, the averaged deflection does not converge exactly to the narrow wedge beam solution (Nevel 1959; Bažant and Li 1994), which is represented by a dashed line in Fig. 3. The discrepancy is minute and the reason for it may be explained by the difference in the definitions of action radii. For infinitely narrow wedge beams floating on water, the action radius is defined as $l = EI/\rho$; and for a plate, the action radius is $L = EI/[\rho(1 - \nu^2)]$. Nevertheless, the difference is so small it can be neglected.

Fig. 4(*a*) shows the contour map of calculated constant deflection contours in a wedge with central angle $\varphi_w = \pi$, in which a rather complicated pattern is displayed. The numbers displayed within the curves are the values of function F, and the number on the right side of the map is the radial coordinate x. For $\varphi_w = \pi/2$, the contour map is shown in Fig. 4(*b*) ($\alpha = 3$; $\alpha_0 = 0.1$). The constant deflection contours are close to straight lines perpendicular to the axis of symmetry of the wedge. This reveals that the narrow wedge-beam approximation proposed by Nevel becomes acceptable when $\varphi_w \leq \pi/2$. However, as is seen from Fig. 4(*a*), the narrow wedge-beam assumption no longer applies for $\varphi_w = \pi$. Comparing Figs. 4(*b*) and 4(*c*), one can understand the effect of the length of radial cracks on the distribution characteristics of the deflection fields. In Fig. 4(*c*), where the radial crack is reduced to $\alpha = 1$, the deformation field beyond the crack tip looks very close to an axisymmetric deformation field, while the defor-

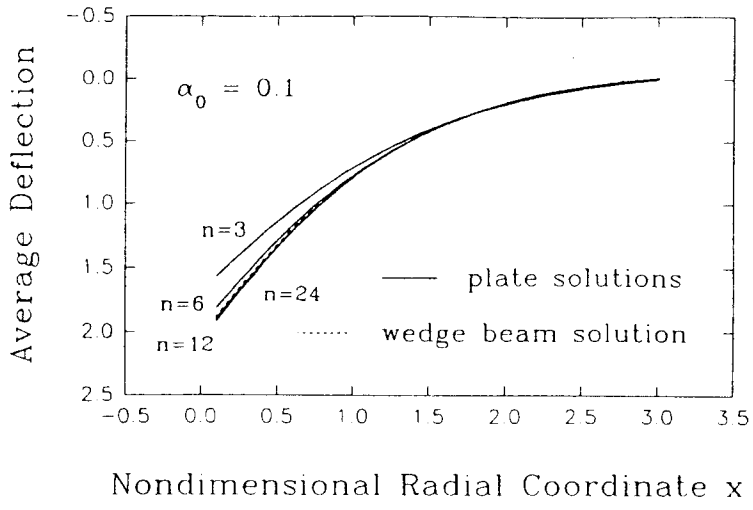

FIG. 3. Average Radial Deflection Profiles of Wedge Plates

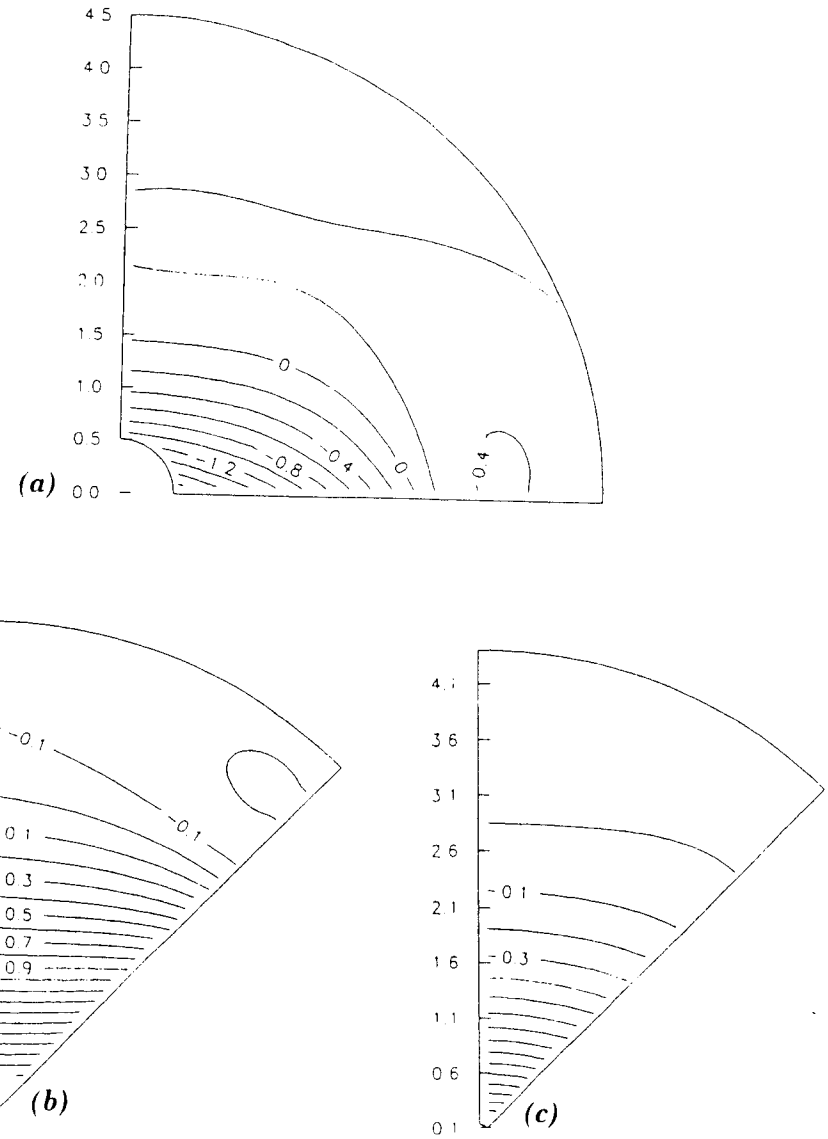

FIG. 4. Deflection Contours: (a) $n = 2$; $\alpha = 3$; (b) $n = 4$; $\alpha = 3$; (c) $n = 4$; $\alpha = 1$

mation within the range of the radial crack looks more like that of a wedge beam. In the neighborhood of the radial crack tip, the deformation pattern is transitional from an axisymmetric plate to a wedge beam.

The nondimensionalized bending moment in polar coordinate system is

$$\tilde{M}_r = \frac{L^2}{D} M_r = -\frac{\partial^2 w}{\partial x^2} - \nu \left(\frac{1}{x} \frac{\partial w}{\partial x} + \frac{1}{x^2} \frac{\partial^2 w}{\partial \theta^2} \right) \tag{7}$$

$\tilde{M}_\theta$ and $\tilde{M}_{r\theta}$ are defined similarly. These moments can be calculated using the central finite difference approximations at internal nodes in the same way as before. For boundary nodes and corner nodes, single-sided finite difference approximations can be used, but the results are of very poor accuracy. This is reflected in sudden jumps of the calculated moment com-

ponents near the boundaries. To avoid this unpleasant feature, the moment values at the boundary nodes as well as at the nodes adjacent to the boundaries are extrapolated from the internal nodes. With this approach, the natural boundary conditions are automatically satisfied, although approximately, as can be seen from the following plots.

Fig. 5(*a*) shows the angular profiles of the moment components in wedges with central angle $\varphi_n = \pi$. Since the central line $\theta = 0$ is a symmetric boundary, $M_{r\theta} = 0$. This condition is a natural result of the fact that the rotation about the x-axis is zero on the boundaries of symmetry. The moment M_θ is zero on the free boundary (the right side of the wedge in the figure). Such a boundary condition is implied in the variational principle and, therefore, is satisfied only approximately when the number of degrees of freedom is finite. Besides, the order of accuracy is lowered due to the adoption of single-sided finite difference approximations. Nevertheless, the calculated M_θ-values are very close to zero in all the cases shown in the figures, except those for very small x. For the case $x = 3$ where the radial crack tip is located, there is a singularity in the moment distribution, which is manifested by the dramatic increases of the moments. It is known that the moment field near the tip of a through-crack in an elastic plate exhibits a singularity of the type $r_c^{-1/2}$ (r_c = distance from the crack tip), which is the same as a crack in a plane, but the angular distribution of the near-tip moment field

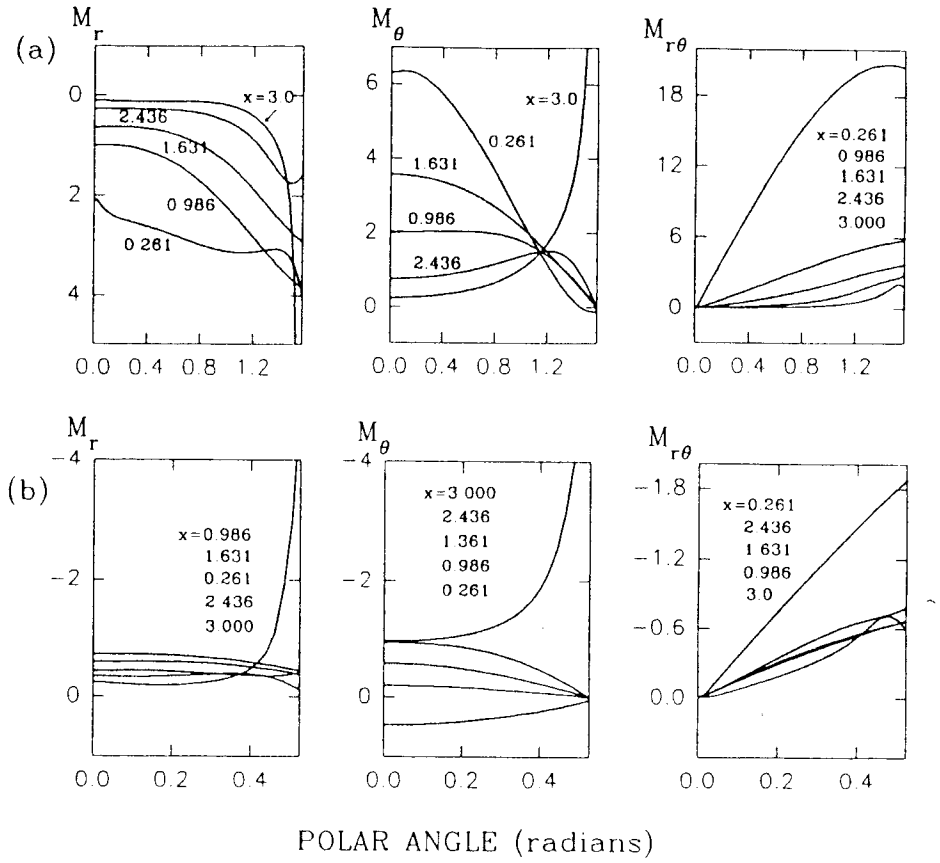

FIG. 5. Circumferential Profiles of Moment Components for: (a) $n = 2$; and (b) $n = 6$

is different [see William (1952) and Paris and Sih (1965)]. It can be shown that the presence of an elastic foundation cannot change the type of singularity. Fig. 5(*b*) shows the moment distributions for wedge angle = $\pi/6$, which is typical of moment distributions for small wedge angles. The moments are nearly uniform, appearing almost as straight lines, which means the deformation field is essentially one-dimensional. It is interesting to note that the radial moment M_r is positive in Fig. 5(*a*), which means that the bottom face of the plate is under tension; however, for small wedge angles the radial moment becomes negative, which means the upper face is under tension, and the wedge behaves similarly to a cantilever.

To clarify the overall distribution of the moment components, the principal bending moments together with their principal directions are calculated. It is seen from the calculations that the maxima and minima of the moments always occur at the radial crack surfaces. Therefore, one needs to examine only the principal moment distributions along the radial cracks. Fig. 6 shows typical distributions of the principal moments and their direction for various radial crack lengths. It demonstrates that when the radial crack is short, there is a strong singularity at the crack tip. The moment is positive and has the direction of M_θ, which indicates that it is the actual cause of the formation of radial cracks. However, as the radial cracks grow, the magnitude of this positive moment gets reduced, which means that a greater load is required to propagate the radial cracks. Meanwhile, as the radial cracks grow, the magnitude of the second principal moment, which is negative, develops a maximum that is located away from the radial crack tip. This negative moment, whose direction is between those of M_r and M_θ, is the cause of the initiation of circumferential cracks, which are nearly perpendicular to the central axis of the wedge. These characteristics of the moment distribution explain why during loading the radial cracks always occur first, and the circumferential cracks will not form until the radial cracks become sufficiently long.

Note also that there is a conspicuous spike in the distributions of both principal moments near the loading edge of the wedge. The nature of such a spike is not totally clear, and it might be an indication of a tendency toward cone-shaped failure. However, the moment distribution is not a good approximation to the true stress distribution near the loading zone of the wedge, because when the thickness of the wedge is of the same order as

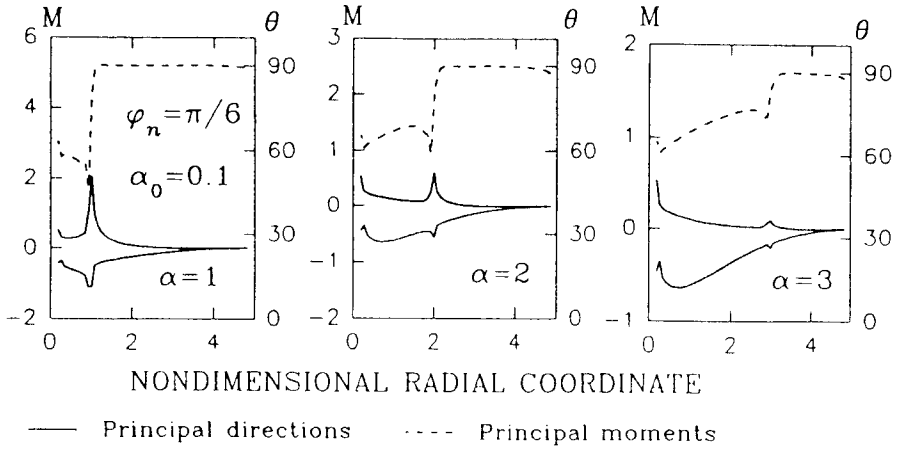

FIG. 6. Distribution of Principal Moments along Radial Cracks (n = 6)

the arc length of the loading edge, the three-dimensional effect must be very significant, making the plate-bending theory no longer suitable. On the other hand, since the plate theory is, nevertheless, the first-order approximation, it is still reasonable to expect that the plate solution provides a correct qualitative, though not necessarily quantitative, estimate of the overall deformation.

ENERGY BALANCE EQUATION FOR RADIAL CRACK PROPAGATION

The basic idea of energy balance during radial crack propagation was presented by Bažant and Li (1994), dealing with one-dimensional analysis. In the present case, the work done by the distributed load varies from point to point, because the deflections at the loading edge of the wedges are not constant. However, the quantity that is of interest is not the distribution of the work, but rather the total work of the applied force. For this purpose, it is sufficient to use the averaged boundary deflection w_0. The averaged boundary deflection can also be written in the form $w_0 = PL^2 f(\alpha_0, \alpha, n)/2\pi D$, where the function $f(\alpha_0, \alpha, n)$ has the same dimension as w. This quantity could further be made nondimensional by comparing the deflection with L. The total work done by the applied load can then simply be written as $Pw_0/2$. The increment of this work due to a change in the radial crack length must be absorbed by the ice sheet to create new crack surfaces, therefore

$$nhG_f = \frac{P^2 L}{4\pi D} f_\alpha(\alpha, \alpha_0, n); \quad f_\alpha(\alpha, \alpha_0, n) = \frac{\partial f(\alpha_0, \alpha, n)}{\partial \alpha} \qquad (8a,b)$$

The only difference between this equation and its one-dimensional counterpart given by Bažant and Li (1994) is that the function f now depends also on n. Function f, which is proportional to the compliance of the structure, is plotted in Fig. 7(*a*) as a function of the radial crack length. The loading zone radius is fixed at $\alpha_0 = 0.01$. The compliance is seen to increase with increasing n. For sufficiently large n, the compliance of the wedge system approaches a constant, which is almost the same as the compliance for the wedge-beam approximation.

As is already known from the one-dimensional analyses, the compliance will reach a maximum and then start to oscillate around this maximum value for sufficiently long radial cracks. The smallest radial crack length, at which

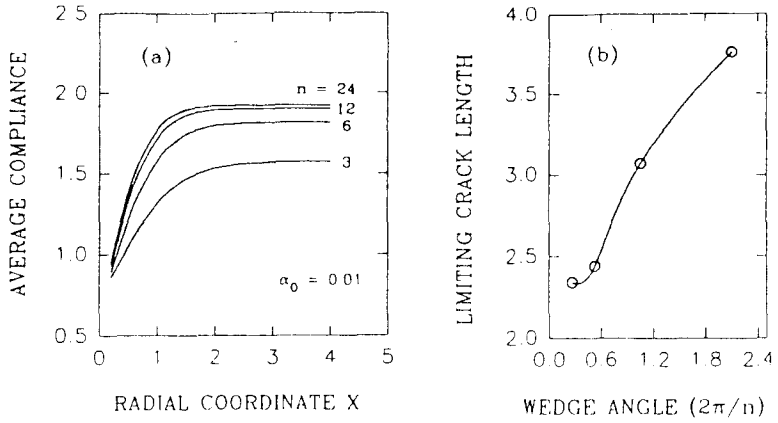

FIG. 7. (*a*) Average Compliance; (*b*) Limiting Radial Crack Length

the compliance derivative is zero, will be called the limiting length of the radial cracks. In one-dimensional analysis, the limiting length is a function of only α_0. In two-dimensional analysis, however, the limiting length depends also on n [Fig. 7(*b*)]. The smaller the n, the longer the limiting length. When n is large enough, the limiting length approaches a constant (about 2.3) that is quite close to the wedge-beam solution (2.02). The causes for this difference are various. In addition to the inevitable numerical error in the two-dimensional analysis, it may also be noted that the two-dimensional model is softer than the wedge-beam model, the limiting length, therefore, should be longer than the wedge-beam solution. Nevertheless, such a difference does not seem to be significant.

THEORY OF INITIAL CRACK SPACING

As noticed by Frankenstein (1963), the number of radial cracks formed in a penetration test is a highly variable quantity. However, for different sizes of the loading device, his tests demonstrated that the number of radial cracks depends on the diameter of penetrator. It is therefore clear that, despite inevitable large random scatter of tests, there is still a deterministic trend. We will discuss this with the understanding that we are seeking only a qualitative theory that is capable of capturing the salient features.

As is well known, the linear elastic fracture mechanics cannot model directly the crack initiation, since when crack length is zero, the energy release rate is also zero. Thus using Griffith's equation of energy balance, the load required to initiate a crack is incorrectly predicted to be infinite. Therefore the strength concept must be used in some form. When the load is uniformly distributed over a circular area of radius α_0, the axisymmetric plate equation can be solved analytically to determine the load P_f at which the first crack occurs (i.e., f_t is reached)

$$P_f = \frac{\pi\alpha_0}{3(1 + \nu)\mathrm{kei}'(\alpha_0)} f_t h^2 = \frac{f_t h^2}{C(\alpha_0)} \tag{9}$$

[see Hertz (1884), Bernstein (1929), and Wyman (1950)]. For $\alpha_0 = 0.01$, 0.06, 0.1, 0.3, 0.6, and 1; $C(\alpha_0) = 3.241$, 2.129, 1.812, 1.135, 0.720, and 0.437. Note the assumption that there is a hole in the ice plate is valid only for calculating the behavior sufficiently far away from the center. As far as the stress in the center is concerned, this assumption is not appropriate anymore.

When (9) becomes satisfied, the ice starts to form cracks. However, the strength theory alone cannot provide the number of radial cracks. Therefore, the energy criterion must be used. First, recall that when the radial crack length approaches zero, so does the energy release rate; and when the radial crack length approaches its limiting length, the energy release rate is reduced to zero again. In other words, the crack propagation is unstable initially, but will become stable when α is large enough. Therefore, once the radial cracks start growing, they will not stop until the energy release rate starts to decrease and the energy balance (8) becomes satisfied for $P = P_f$. Such an equation can be written in a nondimensional form as

$$\frac{n}{f_\alpha(\alpha_0, \alpha, n)} = \frac{L}{l_0} \frac{3(1 - \nu^2)}{\pi C^2(\alpha_0)} \tag{10}$$

where $l_0 = EG_f/f_t^2$ = characteristic size of the process zone of ice.

For each given n (and α_0 as well, of course), (10) makes it possible to determine the initial radial crack length α, which will henceforth be denoted as α_f. However, α_f is generally different for different n. To determine n we need one more relation. The additional relation can be obtained by considering the finite energy release caused by a sudden crack length jump from zero to α_f, which is accompanied by an increase of deflection under the constant load. It is convenient to consider complementary energy, and then this change of energy must be calculated at constant load. The energy released must be consumed by creating the crack surfaces, and so $[f(\alpha_0, \alpha_f, n) - f(\alpha_0, \alpha_0, n)]P_f^2L^2/4\pi D = nL\alpha_f hG_f$, or in the nondimensional form

$$\frac{n}{q(\alpha_0, \alpha_f, n)} = \frac{\alpha_f n}{f(\alpha_0, \alpha_f, n) - f(\alpha_0, \alpha_0, n)} = \frac{3(1 - \nu^2)}{\pi C^2(\alpha_0)} \frac{L}{l_0} \tag{11}$$

The average energy release equation [(11)] and the energy release equation [(10)] can be simultaneously satisfied if and only if the function q is equal to f_α, which occurs when q reaches its maximum. Functions f_α and q are plotted in Fig. 8 for different n and $\alpha_0 = 0.1$. It can be seen that there is only one root in the entire range. The maximum of q is always smaller than the maximum of f_α. Denoting the maximum value of $q(\alpha_0, \alpha, n)$ as

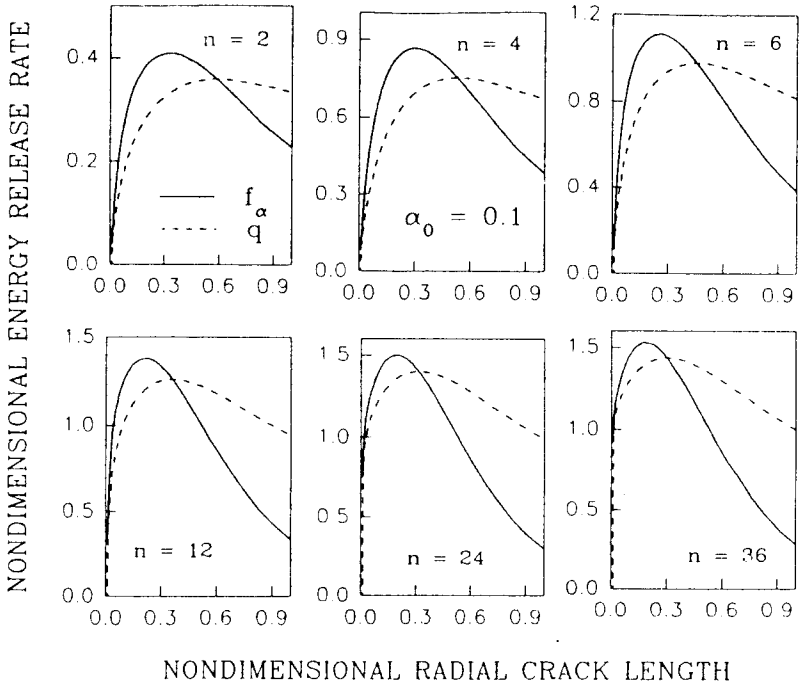

FIG. 8. Tangent Slope f_α and Secant Slope q of Compliance ($\alpha_0 = 0.1$)

TABLE 1. Function Q and n/Q

α_0	n	2	3	4	5	6	8	12	24	36
0.1	Q	0.358	0.580	0.751	0.880	0.978	1.113	1.256	1.397	1.433
0.1	n/Q	5.585	5.175	5.325	5.682	6.135	7.186	9.553	17.18	25.12
0.01	Q	0.339	0.569	0.741	0.867	0.962	1.091	1.223	1.348	1.379
0.01	n/Q	5.893	5.271	5.400	5.767	6.236	7.333	9.732	17.80	26.11

$Q(\alpha_0, n)$, which is listed in Table 1, we can rewrite the energy release rate equation [(10)] as

$$\frac{n}{Q(\alpha_0, n)} = \frac{L}{l_0} \frac{3(1 - \nu^2)}{\pi C^2(\alpha_0)} \tag{12}$$

Experiments (Frankenstein 1963) showed that n increases with increasing punch size, and this trend is indeed captured by (12): because α_0 increases with punch size, whereas $C(\alpha_0)$ decreases with α_0, the final result is an increase in the right-hand side of the equation, and thus an increase in n. More specifically, in Frankenstein's tests, $\alpha_0 \approx 0.06$ for the small punch size and $\alpha_0 \approx 0.6$ for the large punch size. The average number of the radial cracks for the small size punch is about 4.6, and for the large punch size about 24. The ratio $n(\alpha_0 = 0.6)/n(\alpha_0 = 0.06)$ is about 5.2. Now, neglecting the differences in L and l_0 for different test sites, we see from (12) that the ratio of the radial crack numbers should be approximately equal to the ratio of $C^2(0.06)/C^2(0.6)$, which is about 8.7, times the ratio $Q(0.6, 24)/Q(0.06, 5)$, which is roughly 1.6. Thus according to (12), the predicted ratio of the radial crack numbers is about 14. Considering the crudeness of the assumptions used in this calculation and the considerable random scatter exhibited by the test data, the predicted value does not seem unreasonable.

The foregoing prediction might be improved by considering l_0. In the large-size tests, the ice plate was a combination of snow and clear ice, whereas in the small-size tests, the ice plate was clear ice. Because l_0 is proportional to the maximum size of the inhomogeneities in the ice, and the inhomogeneities in the clear ice are finer than those in the snow ice, l_0 for the mixed snow and clear ice must be larger than that for the clear ice. The prediction should be multiplied by the ratio of l_0 (clear ice) over l_0 (snow and clear ice), which should bring the predicted value closer to the measured value, 5.2.

It is also noted that the smallest value of the right-hand side of (12) is zero, while the left-hand side has a minimum, denoted as $U(\alpha_0)$, which is larger than zero and occurs at $n = 3$, as can be seen from Table 1. Then, through (12), one can define the threshold length L_0 as

$$L_0 = \frac{\pi l_0}{3(1 - \nu^2)} C^2(\alpha_0) U(\alpha_0) \tag{13}$$

When the action length L is smaller than L_0, no radial cracks form during loading, and the only way an ice plate may fail is by a conic crack under the load. For instance, for an ice sheet with $l_0 = 0.2$ m and $\alpha_0 = 0.1$, $L_0 = 3.91$ m. When h is measured in meters, the action distance L can be related to h as $L \approx 16h^{3/4}$; thus $h_0 \approx 0.15$ m. Note that the aforementioned threshold value is defined for constant α_0. It is easy to show that even at constant a_0, there is still a lower limit for h [Fig. 9(a)], because function C approaches infinity as a logarithmic function of h. The foregoing equation can also be used to define a lower limit for the punch radius a_0 under the condition of constant h, in which case L_0 is given and the minimum α_0 is to be found through (12) [Fig. 9(b)]. According to this theory, the larger the thickness h, the smaller the a_0. Whether this is true should be confirmed by future experiments.

Eq. (12) can be used directly to find L, and thus also h, that corresponds to a given n. However, we are often interested in the reverse problem: to determine n for a given h. It is natural to expect that for an arbitrarily given

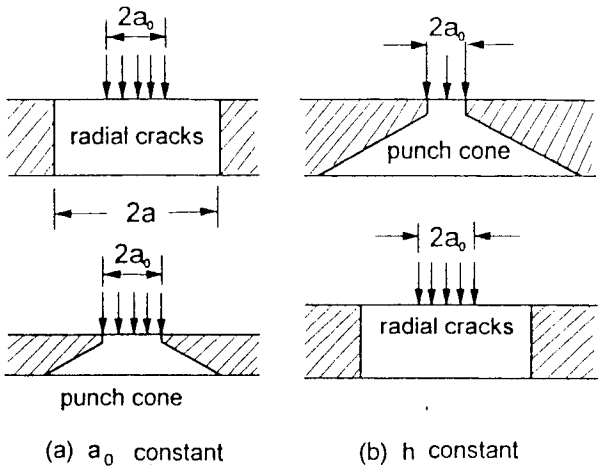

FIG. 9. Change of Failure Mechanism for: (a) Constant a_0; and (b) Constant h

h there might be no n that satisfies the equation, because h is a continuous quantity whereas n is not. Physically, when there is no n that can satisfy (12), which is an energy balance equation, some of the assumptions that lead to (12) must be invalid. Although it is assumed that the radial cracks are equally spaced and have equal length, in reality this might not be true: the radial crack spacing and length might be uneven due to inevitable inhomogeneities in the ice. Although it is assumed that all potential energy is transferred into crack formation, in reality this becomes impossible if some of the energy is converted into kinetic energy during crack jumping. In other words, (12) gives only a simplified picture of a very complicated physical phenomenon. Therefore, whenever (12) cannot be satisfied, we simply pick, for a given h, a value n that makes the unbalance of (12) the smallest.

Nevertheless, some questions remain unsolved. Using the experimental data of Frankenstein, one can determine l_0 indirectly through (12). The results are $l_0 = 0.2$ m for clear ice and $l_0 = 0.6$ m for snow and clear ice. These values seem to be a magnitude too large. The problem may be related to one of our basic hypotheses, which assumes the radial crack to be totally open during loading. According to Frankenstein (1963), the radial cracks are always closed at the top surface of the ice plate, and the crack surface will not open until the applied load is removed. However, detailed consideration would require a three-dimensional analysis, which is beyond the scope of this paper. Once suitable test data become available, this question should be studied further.

The argument that led to (12) for determining the angular crack spacing represents a refinement and extension of the approximate argument used by Bažant and Ohtsubo (1979) to determine the initial spacing of the parallel cooling cracks in a half-plane [see also Bažant and Cedolin (1991), chapter 12].

SIZE EFFECT

Previous studies (Bažant 1991, 1992) yielded a result at first perplexing: for elastic plates of different thickness h, resting on a Winkler foundation, the nominal stress $\sigma_N = P/h^2$ required to propagate geometrically similar

cracks is, according to LEFM, proportional to $h^{-1/8}$. This seems to conflict with the fact that in LEFM the size effect is of the type $\sigma_N \sim (\text{size})^{-1/2}$, and h is the only geometric dimension (i.e. size) for the infinite plate. The explanation is that the problem is two-dimensional, and size h is measured in the third dimension; thus h represents merely a parameter, not an actual dimension in the (x, y) domain in which the boundary-value problem is mathematically defined. The characteristic dimension in the plane (x, y) is not geometric, but is provided by L, and indeed, in terms of L the LEFM size effect is of the type $\sigma_N \sim L^{-1/2}$ (Bažant 1992; Bažant and Li 1992).

Except for the initial crack formation, the radial cracks grow stably under load control, which means the applied load P needs to be increased as the radial cracks grow longer. P_{max} is reached when circumferential cracks initiate. The crack initiation is not governed by LEFM but by the strength theory, which causes no size effect (i.e. $\sigma_N \sim L^0$). But, as shown, the maximum bending stress that causes the initiation of circumferential cracks occurs when the radial cracks become sufficiently long; therefore the size effect is a combination of LEFM size effect and strength size effect.

Fig. 10(*a*) shows the magnitudes of the nondimensional maximum moment M_{max} as a function of the wedge angle φ_n for different α_0. When the wedge angle becomes very small, M_{max} approaches some constant that depends only on α_0. The load required to initiate the circumferential cracks (P_{max}) is significantly higher than the load required to initiate the radial cracks (P_f) given by (9). The ratio $p = P_{max}/P_f = \pi C(\alpha_0)/3M_{max}$ (which is proportional to the nominal stress σ_N) is plotted in Fig. 10(*b*), which can be seen to be typically larger than 2. Without applying fracture mechanics, the predicted maximum load would be P_f, which would be much too conservative.

The size effect on nondimensional nominal stress σ_N ($= P_{max}/h^2 f_t$) depends on how the similarity is defined. If it is defined so that α_0 is constant for varying h, then there is no size effect if the effect of bending modulus and of changing crack number n are neglected, as is shown in Fig. 11(*a*). In the calculation it is assumed that $l_0 = 0.2$ m and $L = 16h^{3/4}$. The size effect due to a change in n under constant α_0 is plotted in Fig. 11(*b*). The

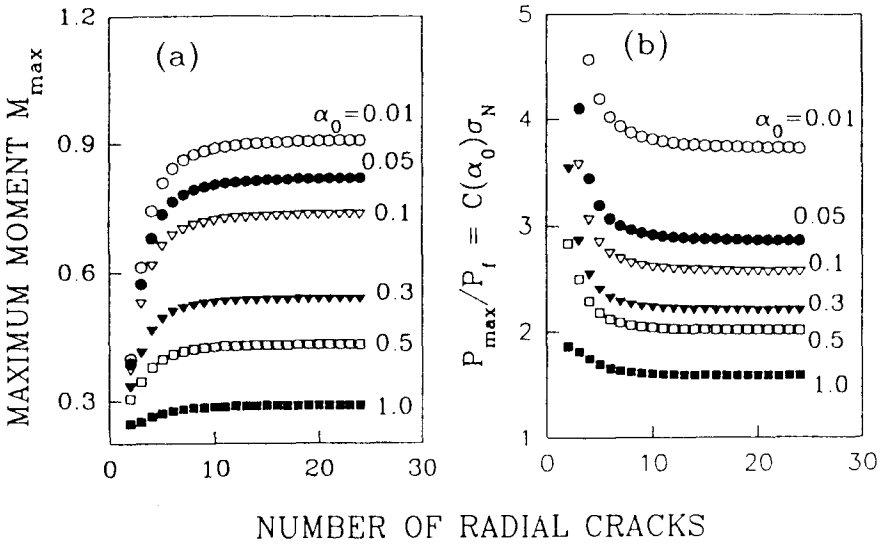

FIG. 10. (*a*) Maximum Moment: and (*b*) Load Factors p

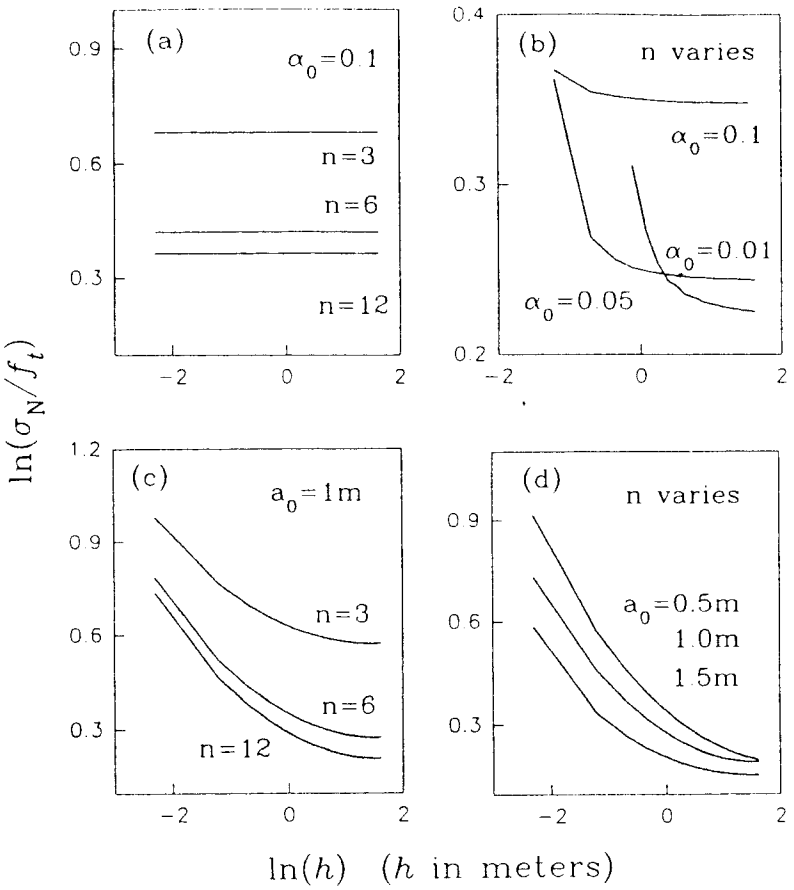

FIG. 11. Size Effect for: (*a*) Constant α_0 and Constant n; (*b*) Constant α_0 and Varying n; (c) Constant a_0 and Constant n; (*d*) Constant a_0 and Varying n

left end of the curves corresponds to the threshold value L_0 as discussed in the previous section.

It may be emphasized that the size effect due to a change in n can be seen only through a two-dimensional analysis. The conclusions in the previous one-dimensional study (Bažant and Li 1994) could not reflect such a size effect, because in the narrow wedge-beam solution the maximum bending moment is independent of the wedge angle, and thus independent of n.

When the ratio a_0/h is kept constant for various h, a reversed size effect is superimposed on the size effect just mentioned. Since $\alpha_0 = (a_0/h)[h(1 - \nu^2)/E]^{1/4}$, α_0 actually increases with h, and we know that when α_0 increases, the maximum value of the nominal stress increases, and thus the size effect gets reversed: the larger h is, the larger σ_N is. However, since the dependence of α_0 on h is very weak in the normal range of thickness, such a reversed size effect can often be neglected. Actually, keeping a_0 constant for all h is the case that is more relevant to the practical problem—an aircraft of a fixed and known contact area landing safely on the ice plate, or a submarine of a fixed and known contact area of its sail penetrating upward through the ice. For this case, α_0 decreases with h, and so the maximum nominal stress decreases with h too, as is shown in Fig. 11(*c*) for several chosen n. This type of size effect has already been discussed by Bažant and Li (1994).

It is interesting to note that even with constant a_0, n still increases with h, because the rate of increase of L is faster than that of function C^2. Thus the overall effect of changing n is to enhance the size effect under the condition of constant a_0, as can be seen from Fig. 11(d).

CONCLUSIONS

1. The variational finite difference method, in which the equilibrium equations for nodal deflections are obtained by differentiating the potential energy approximated by finite differences, is an effective way to solve an elastic plate on elastic foundation. The energy release rate is obtained by differentiating the potential energy as a function of the radial crack length.

2. Based on the assumptions of linear elastic fracture mechanics and the plate bending theory, our numerical calculations confirm that the load from the penetrating object (a punch) distributed along a small (but not too small) circle causes propagation of radial cracks, and that the maximum load is reached at the initiation of circumferential cracks whose radial distance is less than the radial crack length. Assuming equal central angles of the radial cracks, one needs to analyze only one-half of an infinite wedge plate between two radial crack lines.

3. Although, as determined previously, the nominal stress (load divided by plate thickness square) required to propagate geometrically similar cracks is proportional to (thickness)$^{-3/8}$, the size effect is modified because: (1) The initiation of the circumferential cracks is governed by the strength limit of ice rather than its fracture energy; and (2) the number of radial cracks varies with the ice-plate thickness.

4. The previously presented simplified one-dimensional solution, in which the radial cracks are considered very dense and the wedge plates are treated as narrow wedge beams (Nevel's approximation), is sufficiently accurate for wedge angles up to $\pi/4$. The error is negligible when the wedge angle is less than $\pi/6$. However, the complicated distribution of the moments can only be obtained through a two-dimensional analysis.

5. As an extention and generalization of a previous idea, a theory for the initial crack spacing is proposed. The idea is that the initial crack number n must satisfy the following three conditions simultaneously: (1) The energy release rate is equal to the fracture energy of the ice; (2) the total energy released suffices to produce the total crack area $\alpha_t hn$; and (3) the applied load is such that the maximum stress before cracking be equal to the tensile strength of the ice. This theory also reveals that for a given nondimensional punch radius $\alpha_0 = a_0/L$ (a_0 = radius of punch size; L = decay length of the plate), there is a threshold thickness below which the ice plate fails by a conic crack. The smaller the α_0, the larger the threshold thickness.

6. Aside from the size effect on the modulus of rupture for bending, there are two factors that affect the final combined size effect: (1) A change in the number n of radial cracks as a function of α_0 and L; and (2) the modification of size effect due to the definition of similarity. If constant α_0 is used to define the similarity, and as long as n is constant, there is no size effect due to a change in thickness. If a_0 is constant, then there is a size effect because α_0 decreases with thickness. The effect of a change in the number of radial cracks is always to enhance the overall size effect.

ACKNOWLEDGMENT

Financial support under grant N00014-91-J-1109 (monitored by Dr. Y. Rajapakse) from the Office of Naval Research to Northwestern University is gratefully acknowledged.

APPENDIX. REFERENCES

Bažant, Z. P., Ohtsubo, R., and Aoh, K. (1979). "Stability and post-critical growth of a system of cooling and shrinkage cracks." *Int. J. Fracture*, Vol. 15, 443–456.

Bažant, Z. P., and Cedolin, L. (1991). *Stability of structures: elastic, inelastic, fracture and damage theories*. Oxford University Press, New York, N.Y.

Bažant, Z. P. (1991). "Large scale thermal bending fracture of sea ice plate." *Rep. 91-3/402t*, Dept. of Civ. Engrg., Northwestern University, Evanston, Ill.

Bažant, Z. P. (1992). "Large-scale fracture of sea ice plates." *Proc., 11th IAHR Int. Ice Symp.*, IAHR, Banff, Alberta, Canada, 991–1005.

Bažant, Z. P., and Li, Y. N. (1994). "Penetration fracture of sea ice plate: simplified analysis and size effect." *J. Engrg. Mech.*, ASCE, 120(6), 1521–1542.

Bernstein, S. (1929). *The railway ice crossing*. Trudy Nauchno-Technicheskogo Komiteta Narodnogo Komissariata Putei, Soobshchenniia, Russia, Vol. 84 (in Russian).

Bushnell, D. (1973). "Finite-difference energy models versus finite-element models: two variational approaches on one computer program." *Numerical and computer methods in structural mechanics*, Fenves et al., eds., Academic Press, New York, N.Y., 292–336.

Forsythe, G. E., and Wason, W. R. (1960). *Finite difference methods for partial differential equations*. Wiley, New York, N.Y.

Frankenstein, E. G. (1963). "Load test data for lake ice sheet." *Tech. Rep. 89*, U.S. Army Cold Regions Research and Engineering Laboratory, Hanover, N.H.

Hall, C. A., and Porsching, T. A. (1990). *Numerical analysis of partial differential equations*. Prentice-Hall, Inc., Englewood Cliffs, N.J.

Hertz, H. (1884). "Über das gleichgewicht schwimmender elastischer Platten [on the equilibrium of floating elastic plates]." *Wiedemann's Annalen der Phys. und Chem.*, Germany, Vol. 22 (in German).

Kerr, A. D. (1975). "The bearing capacity of floating ice plates subjected to static or quasi-static loads—a critical survey." *Res. Rep. 333*, U.S. Army Cold Regions Research and Engineering Laboratory, Hanover, N.H.

Nevel, D. E. (1958). "The theory of narrow infinite wedge on an elastic foundation." *Trans.*, Engineering Institute of Canada, 2(3).

Nevel, D. (1965). "A semi-infinite plate on an elastic foundation." *USA ARREL Res. Rep. 136; AD 616313*, ARREL.

Paris, P., and Sih, G. C. (1965). "Stress analysis of cracks." *Fracture Toughness and Its Applications; STP No. 381*, ASTM, Philadelphia, Pa., 30.

Selvadurai, A. P. S. (1979). *Elastic analysis of soil-foundation interaction*. Elsevier Scientific Publ. Co., New York, N.Y.

Westergaard, H. M. (1923). "Om beregning af plader paa elastisk underlag med saerligt henblik paa sporgsmaalet om spaendinger i betonveje." *Ingenioren*, Copenhagen, Denmark, No. 42 (in Danish).

Williams, M. L. (1952). "Surface stress singularities resulting from various boundary conditions in angular corners of plates under bending." *Proc., 1st U.S. Nat. Congress of Appl. Mech.*, 325.

Wyman, M. (1950). "Deflections of an infinite plate." *Can. J. of Res.*, Vol. A28.